A&A manuscript no.
(will be inserted by hand later)

Your thesaurus codes are:
12(09.13.2; 02.12.3; 11.17.1; 11.17.4 Q0000–2620)

ASTRONOMY AND ASTROPHYSICS
July 29, 2000

UVES observations of QSO 0000–2620 : Molecular hydrogen abundance in the damped Lyα system at $z_{\rm abs} = 3.3901^\star$

S. A. Levshakov[1], **P. Molaro**[2], **M. Centurión**[2], **S. D'Odorico**[3], **P. Bonifacio**[2], **and G. Vladilo**[2]

[1] Department of Theoretical Astrophysics, Ioffe Physico-Technical Institute, 194021 St. Petersburg, Russia
[2] Osservatorio Astronomico di Trieste, Via G.B. Tiepolo 11, 34131, Trieste, Italy
[3] European Southern Observatory, 85748 Garching bei München, Germany

Received 24 May 2000 / Accepted 00 July 2000

Abstract. We have discovered molecular hydrogen in a fourth quasar damped Lyα system (hereafter DLA). The UVES spectrograph on the 8.2m ESO Kueyen telescope has allowed the detection of H_2 in gas with low metallicity, $Z/Z_\odot \simeq 10^{-2}$, and high neutral hydrogen column density, $N(\text{H I}) \simeq 2.6 \times 10^{21}$ cm^{-2}, at redshift $z_{\rm abs} = 3.3901$ toward QSO 0000–2620. The measured H_2 fractional abundance of $f(\text{H}_2) \simeq 4 \times 10^{-8}$ is lower than a typical value for Galactic interstellar clouds of high $N(\text{H I})$ column density by a factor of $(2-3) \times 10^6$. Since H_2 molecules are formed efficiently on dust grains, it implies that the dust condensation in this DLA is negligible, and hence the abundances derived from metal absorption lines are the actual ones. The obtained $f(\text{H}_2)$ value leads to an estimate of the dust number density of $\langle n_{\rm d}\rangle_{\rm DLA} \sim 10^{-3} \langle n_{\rm d}\rangle_{\rm ISM}$, which is consistent with the dust-to-gas ratio $\tilde{k} \leq 1.6 \times 10^{-3}$ derived independently from the [Cr/Zn] and [Fe/Zn] ratios.

Key words: line: profiles – ISM: molecules – quasars: absorption lines – quasars: individual: Q0000–2620

1. Introduction

In this work we continue our chemical composition analysis of the $z_{\rm abs} = 3.3901$ damped Lyα system from the spectrum of the bright quasar Q0000–2620 (V = 17.5, $z_{\rm em} = 4.108$) observed with the UVES spectrograph (Dekker et al. 2000) at the 8.2m ESO Kueyen telescope during the first commissioning in October 1999 (Molaro et al. 2000, hereafter Paper I).

Paper I was mainly concerned with precise measurements of the oxygen and zinc abundances. The obtained O and Zn metallicities together with other α-chain and iron-peak element abundances present a pattern of a galactic chemical composition different from that of the Milky Way. In particular, it was found that the relative abundances of α-chain and iron-peak elements, [O,Si,S/Cr,Fe,Zn], are significantly lower than analogous ratios in Galactic stars with comparable metallicities. The measured Zn abundance, [Zn/H] $= -2.07 \pm 0.1$ dex[1], is the lowest among DLAs, which implies that the $z_{\rm abs} = 3.3901$ intervening galaxy is in the early stages of its chemical evolution. This suggestion is consistent with the similar abundances found for the volatile (Zn) and refractory (Cr and Fe) elements, [Cr/H] $= -1.99 \pm 0.1$ dex and [Fe/H] $= -2.04 \pm 0.1$ dex, which means, in turn, that the Cr and Fe atoms may not be locked up in dust grains and that the dust-to-gas ratio in this DLA may be much lower if compared with Galactic diffuse clouds with the same neutral hydrogen column densities, $N(\text{H I}) \simeq 2.5 \times 10^{21}$ cm^{-2}.

The low dust-to-gas ratio in this system suggested in Paper I is consistent with the absence of significant H_2 absorption at $z_{\rm abs} = 3.3901$ in the Lyman $\text{B}^1\Sigma^+_{\rm u} \leftarrow \text{X}^1\Sigma^+_{\rm g}$ and Werner $\text{C}^1\Pi^\pm_{\rm u} \leftarrow \text{X}^1\Sigma^+_{\rm g}$ bands (Levshakov et al. 1992, hereafter LCFB) as well as with the absence of CO lines from the fourth positive band $\text{A}^1\Pi \leftarrow \text{X}^1\Sigma^+$ (Lu et al. 1999).

It should be noted that in the Galactic interstellar medium, sightlines with $N(\text{H I}) \gtrsim 10^{21}$ cm^{-2} show high fractional abundances of hydrogen in molecular form, $f(\text{H}_2) \sim 0.1$ (Savage et al. 1977), where $f(\text{H}_2) = 2N(\text{H}_2)/N(\text{H})$ with $N(\text{H}_2)$ and $N(\text{H})$ being the total column densities of H_2 and H, respectively. Such molecular clouds with $N(\text{H}_2) \gtrsim 10^{19}$ cm^{-2} provide an effective self-shielding in the Lyman and Werner bands preventing UV photons from penetrating the interior of the clouds and thus lowering photodissociation rates of H_2 and CO molecules.

In contrast with the ISM diffuse clouds, molecular hydrogen in DLAs shows different behavior. Namely, we do not observe a pronounced transition from low to high molecular fractions at total hydrogen column density near 5×10^{20} cm^{-2} as found in the Milky Way disk by Savage et

Send offprint requests to: S. A. Levshakov

* Based on public data released from the UVES commissioning at the VLT Kueyen telescope, European Southern Observatory, Paranal, Chile.

Correspondence to: lev@astro.ioffe.rssi.ru

[1] Using the customary definition [X/H] = log (X/H) – log (X/H)$_\odot$

al. (1977). The first H_2 system identified at $z_{abs} = 2.8112$ toward Q0528–250 by Levshakov & Varshalovich (1985) gives very low amount of H_2, $f(H_2) \simeq 5.4 \times 10^{-5}$, while $N(\text{H I}) \simeq 2.2 \times 10^{21}$ cm^{-2} (see also Srianand & Petitjean 1998 and references cited therein). However, the second and the third H_2 systems found at $z_{abs} = 1.97$ toward Q0013–004 (Ge & Bechtold 1997) and at $z_{abs} = 2.34$ toward Q1232+0815 (Ge et al. 2000) show high H_2 abundances, $f(H_2) \simeq 0.22$ and 0.07, respectively (the corresponding neutral hydrogen column densities are equal to 6.4×10^{20} cm^{-2} and 8.0×10^{20} cm^{-2}). Other DLAs have led so far only to upper limits, $f(H_2) \lesssim 2 \times 10^{-4}$, with the lowest bound of 9×10^{-7} at $z_{abs} = 2.47$ toward Q1223+17 (Bechtold 1999).

LCFB derived an upper limit of $f(H_2) < 3 \times 10^{-6}$ for the DLA at $z_{abs} = 3.3901$ toward Q0000–2620. The correlation between the H_2 fractional abundance and the [Cr/Zn] ratio found by Ge & Bechtold (1999; see their Fig. 1) suggests that $f(H_2) \lesssim 10^{-7}$ if [Cr/Zn] ~ 0, as measured in Paper I. This motivated us to search for the H_2 transitions in the UVES spectrum already discussed in Paper I. We show below that the S/N of this spectrum is indeed adequate to measure H_2, thus making this absorber the fourth one for which such a measure is available.

2. Data analysis and Results

2.1. Observations and the H_2 identification

Spectroscopic observations of Q0000–2620 are described in detail in Paper I. The spectrum was obtained with the rms uncertainty of the wavelength calibration $\delta\lambda \leq 0.6$ km s^{-1}, the velocity resolution of FWHM $\simeq 6$ km s^{-1} (the corresponding bin size equals 2.4 km s^{-1}) and the signal-to-noise ratio of S/N $\simeq 40$ (per pixel) in the range $\lambda\lambda = 4605 - 4615$ Å which allows us to detect the L(4-0)R(1) line at the expected position, $\lambda_{obs} = 4609.4$ Å. The absence of this line in the 1 Å resolution spectrum obtained with the Multiple Mirror Telescope (MMT) in 1988 (LCFB) has led to the limit $W_{rest} < 114$ mÅ (3σ) for the equivalent width of the L(4-0)R(1) line. The UVES spectrum shown in Fig. 1a provides $W_{rest} \simeq 6$ mÅ. The local continuum level in the vicinity of the L(4-0)R(1) line was additionally controlled by the optical depth value of the Lyman-limit discontinuity ($\tau_c = 0.003$) from the metal system at $z_{abs} = 4.061$ (Savaglio et al. 1996). This is illustrated in Fig. 2 where the estimated continuum level between 4555 Å and 4660 Å is shown by the dotted line. The vertical line at $\lambda = 4614.39$ Å marks the Lyman-limit position for the $z_{abs} = 4.061$ system. The expected optical depth in the continuum at $\lambda = 4609$ Å is equal to $\tau_{4609} = \tau_c\,(4609/4614)^3 \simeq 0.003$.

We have thoroughly investigated all possible coincidences of the L(4-0)R(1) position with metal absorptions from other systems observed toward Q0000–2620. Only one such case was found. The position of the C IIλ903.6235

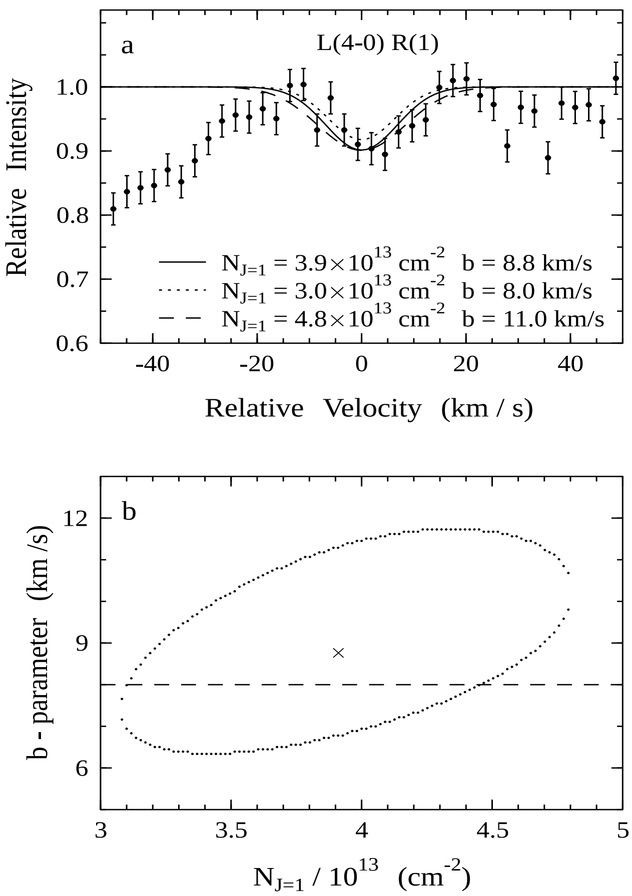

Fig. 1. (**a**) – Observed normalized intensities (dots with error bars) vs radial velocities given relative to $z_{abs} = 3.390127$. The rest frame wavelength of the L(4-0)R(1) line and its oscillator strength (1049.958 Å and 0.0160, respectively) were taken from Morton & Dinerstein (1976). Smooth lines are the synthetic spectra obtained from the χ^2 minimization as described in the text. (**b**) – Confidence region in the '$N_{J=1}(H_2) - b$' plane. The contour above the dashed horizontal line represents 70% accepted confidence level. The horizontal line restricts b-values which are less than the lowest 1σ boundary for the b-value of the heaviest element from the $z_{abs} = 3.3901$ system, $b_{\text{Zn II}} \geq 8.0$ km s^{-1} (Paper I). The cross marks the point of maximum likelihood for the best fit shown by the solid line in panel **a**

($f_{abs} = 0.168$) line from the metal system at $z_{abs} = 4.10106$ detected by Savaglio et al. (1997) differs from the center of the L(4-0)R(1) line by only -0.7 km s^{-1}. If the feature observed ($W_{obs} = 26$ mÅ) were due to this C II absorption, we would obtain $W_{rest} = 5$ mÅ and $N(\text{C II}) = 4.27 \times 10^{12}$ cm^{-2} using the linear part of the curve of growth. This would imply an abundance [C/H] $\simeq +1.68$ which is unlikely, due to the high redshift of the absorber. We remark that even assuming a solar carbon abundance, [C/H] = 0, and the unrealistic suggestion that all carbon is in the C II form (Savaglio et al. have detected C IV in this system which is not a DLA) we find that $W_{obs}(\text{C II}) = 0.5$ mÅ. This result implies that the C II ab-

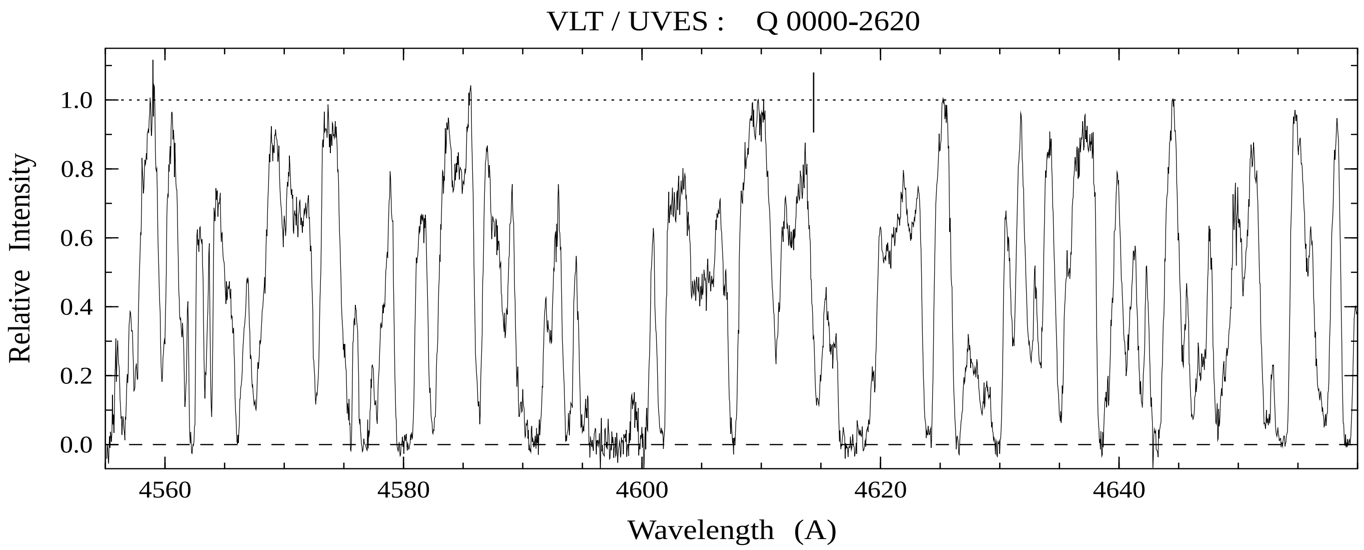

Fig. 2. A portion of the Q 0000–2620 spectrum in the vicinity of the H_2 L(4-0)R(1) line ($\lambda_{\rm obs} = 4609.4$ Å). The Lyman-limit discontinuity of the metal system at $z_{\rm abs} = 4.061$ ($\tau_c = 0.003$) is marked by the vertical line (see text for details)

sorption at $z_{\rm abs} = 4.10106$ does not affect significantly the H_2 profile.

The identification of other H_2 transitions from the Lyman and Werner bands is hampered by blending with numerous Lyα forest lines. Therefore, to obtain quantitative estimates of the total molecular hydrogen column density and the excitation temperature, $T_{\rm ex}$, we choose small continuum 'windows' which are less obscured by the Lyα forest absorption features and where some H_2 lines are expected. The following is a description of the adopted procedure.

2.2. Column densities and the excitation temperature

The inferred H_2 column density, $N(H_2) = \sum_J N_J$, depends on the populations of the first rotational levels ($J = 0, 1, 2, ...$) in the ground state, $T_{\rm ex}$, and the Doppler b-parameter. In thermal equilibrium, the ratio of the column densities N_J is given by

$$\frac{N_J}{N_0} = \frac{g_J}{g_0} \exp\left[-\frac{B_v J(J+1)}{T_{\rm ex}}\right] , \quad (1)$$

where the statistical weight of a level J is $3(2J+1)$ for odd J and $(2J+1)$ for even J (the ortho- and para-H_2, respectively), and the constant $B_v = 85.36$ K for the vibrational ground state.

The central optical depth, τ_0, for the resolved absorption line is determined by (e.g., Spitzer 1978)

$$\tau_0 = 1.497 \times 10^{-15} \lambda_0 f_{\rm abs} \frac{N}{b} , \quad (2)$$

where $f_{\rm abs}$ is the oscillator strength of the transition, λ_0 its wavelength in Å, N the total column density in cm^{-2}, and b the Doppler parameter in km s^{-1}. For the H_2 lines, wavelengths and oscillator strengths were taken from the list of Morton & Dinerstein (1976).

To estimate the ortho-H_2 column density, N_1, and the b-parameter, we fit theoretical Voigt profiles to the observed intensities via χ^2 minimization using a fixed value of $z_{\rm abs} = 3.390127$ which corresponds to the redshift of the isolated Ni IIλ1709 absorption line (Paper I). During the fitting procedure the theoretical profiles are convolved with a Gaussian of the instrumental width of 6 km s^{-1}. We tried to find a satisfactory result with the reduced χ^2 per degree of freedom of $\chi^2_{\rm min} \leq \chi^2_{\nu,0.30}$ (where $\chi^2_{\nu,0.30}$ is the expected χ^2 value for ν degrees of freedom at the credible probability of 70 %). We used the velocity range $|\Delta v| \leq 20$ km s^{-1} where we have $\chi^2_{14,0.30} = 1.159$. The best fit with $\chi^2_{\rm min} = 0.80$ is shown in Fig. 1a by the solid curve, whereas points with error bars give the normalized intensities (the corresponding S/N $\simeq 40$).

The best solution yields $N_1 = 3.9 \times 10^{13}$ cm^{-2} and $b = 8.8$ km s^{-1}. Of course, our analysis gives a certain range for allowable N_1 and b. This is shown in Fig. 1b, where the 70 % confidence region for this pair of physical parameters is restricted by the upper part of the ellipse over the line $b = 8$ km s^{-1}. The second part of the ellipse under this horizontal dashed line may be excluded from consideration since the b-value of the heaviest element Zn II equals 9.3 ± 1.3 km s^{-1} (Paper I), otherwise one would have a zone where $b_{H_2} < b_{\rm Zn\,II}$. The cross in Fig. 1b marks the point of maximum likelihood for the best fit. Two additional curves in Fig. 1a (dotted and dashed) show the L(4-0)R(1) profiles for the limiting values of $N_1 = 3.0 \times 10^{13}$ cm^{-2} and 4.8×10^{13} cm^{-2}, respectively. Both of them have $\chi^2_{\rm min} = 1.06$. To summarize, we set $N_1 = (3.9 \pm 0.9) \times 10^{13}$ cm^{-2} and $b_{H_2} = 8.8^{+3.0}_{-0.8}$ km s^{-1}.

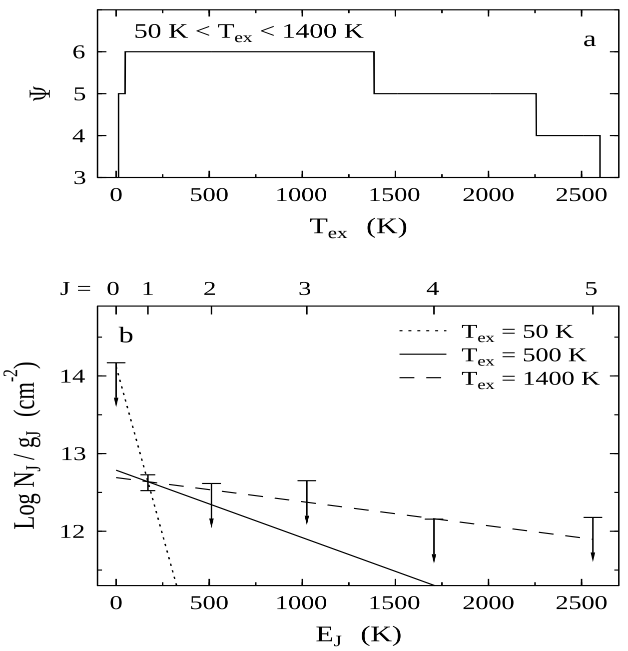

Fig. 3. (**a**) – Ψ- function defined in Eq. (4) vs the excitation temperature $T_{\rm ex}$. The values of $\Psi = 6$ restrict the range for acceptable $T_{\rm ex}$ as illustrated in panel **b**. (**b**) – Population density in H_2 rotational levels observed in the $z_{\rm abs} = 3.3901$ system. The column density $N_{J=1}$ for H_2 molecules in level $J = 1$ per cm^2 (or the upper limits of N_J for $J = 0, 2-5$), divided by the statistical weight, g_J, is plotted on a logarithmic scale against the excitation energy, E_J, in K. The corresponding values of J are shown in the horizontal scale at the top. The points have been fitted with one straight line using Eq.(4), and a value of $T_{\rm ex}$, obtained from the usual Boltzmann formula. The shown straight lines correspond to $T_{\rm ex} = 50, 500$, and 1400 K

Let us now turn to the estimation of the total $N(H_2)$. As mentioned above the total molecular hydrogen column density depends on $T_{\rm ex}$. Typical ISM diffuse molecular clouds have a mean $(J = 0)/(J = 1)$ excitation temperature of $\langle T_{01} \rangle = 77 \pm 17$ K, with the bulk lying in the range from 45 to 128 K (Savage et al. 1977). The excitation temperature T_{01} reflects the relative populations of $J = 0$ and 1 rotational levels which are controlled by thermal particle collisions. Therefore T_{01} is approximately equal to the kinetic temperature, $T_{\rm kin}$, of the cloud. The population of the higher rotational levels are established by collisions, UV pumping and radiative cascades after photo-absorption to the Lyman and Werner bands and thus $T_{\rm ex}$ for the higher levels may differ from T_{01} in dense molecular clouds (see, e.g. a review by Dalgarno 1976). However, for tenuous clouds, a unique temperature for all the levels can be found suggesting that the rotational population could be dominated by collisions in a gas whose kinetic temperature is near $T_{\rm ex}$. For example, the excitation temperature of 1120 ± 80 K toward ζ Pup was measured for $J = 0 - 7$ by Morton & Dinerstein (1976).

There is also a tendency toward low excitation temperatures $T_{\rm ex} \sim 100$ K for the clouds with $f(H_2) > 0.05$, whereas clouds with $f(H_2) < 0.05$ tend to higher $T_{\rm ex}$ (Spitzer & Jenkins 1975). Note that spin temperatures $\gtrsim 10^3$ K have been measured in DLAs with $N(\text{H I}) > 10^{21}$ cm^{-2} for which 21 cm line measurements are available (de Bruyn et al. 1996, Carilli et al. 1996). These measurements assume, however, a similar covering factor of the optical and radio background source.

The excitation temperature can be estimated directly from the comparison of the population density in H_2 rotational levels or indirectly from the thermal width of the H_2 lines assuming that $T_{\rm ex}$ is approximately equal to the kinetic temperature of the cloud. For the DLA in question, we know exactly that the line widths do not reflect the thermal motion since all species from the lightest H_2 to the heaviest Zn show approximately the same b-values (see Paper I). We also have not accurate measurements of N_J for different J. Therefore, to estimate $T_{\rm ex}$ we applied another method.

We choose the continuum 'windows' which are sensitive to the presence of the H_2 absorption and set upper limits for N_J using the inequality

$$\tau_0^{H_2} < \tau_0^{\rm obs} , \tag{3}$$

with $\tau_0^{\rm obs}$ being the observed limit at the expected H_2 transition and $\tau_0^{H_2}$ the quantity calculated from (2). In this estimations we used $b_{H_2} = 8.8$ km s^{-1}. The obtained limits are depicted by short horizontal bars in Fig. 3b.

Now we know the upper limits $N_J^{\rm lim}$ for $J = 0, 2, 3, 4, 5$ and the measured N_1 value. To estimate $T_{\rm ex}$ consider the following function :

$$\Psi(T_{\rm ex}) = \sum_J \psi_J , \tag{4}$$

where for $J = 0, 2, 3, 4, 5$ we have

$$\psi_J = \begin{cases} 1, \text{ if } N_J^{\rm calc} < N_J^{\rm lim} \\ 0, \text{ otherwise} , \end{cases}$$

and for $J = 1$

$$\psi_J = \begin{cases} 1, \text{ if } |N_1^{\rm calc} - N_1| \le \delta N \\ 0, \text{ otherwise} , \end{cases}$$

where $\delta N = 0.9 \times 10^{13}$ cm^{-2}.

Here $N_J^{\rm calc}$ is calculated as

$$N_J^{\rm calc} = N_1 \frac{g_J}{g_1} \exp\left[-\frac{B_v J(J+1)}{T_{\rm ex}} + \frac{2B_v}{T_{\rm ex}} \right] . \tag{5}$$

It follows from the definition of $\Psi(T_{\rm ex})$ that the allowable range for $T_{\rm ex}$ should correspond to the maximum value of Ψ (here equals 6). The shape of Ψ as function of $T_{\rm ex}$ is shown in Fig. 3a which readily gives the range 50 K $< T_{\rm ex} <$ 1400 K. The range is rather wide since we have only one unblended H_2 line. It should be noted, however, that the obtained limits do not contradict the above mentioned observational estimations of $T_{\rm ex}$.

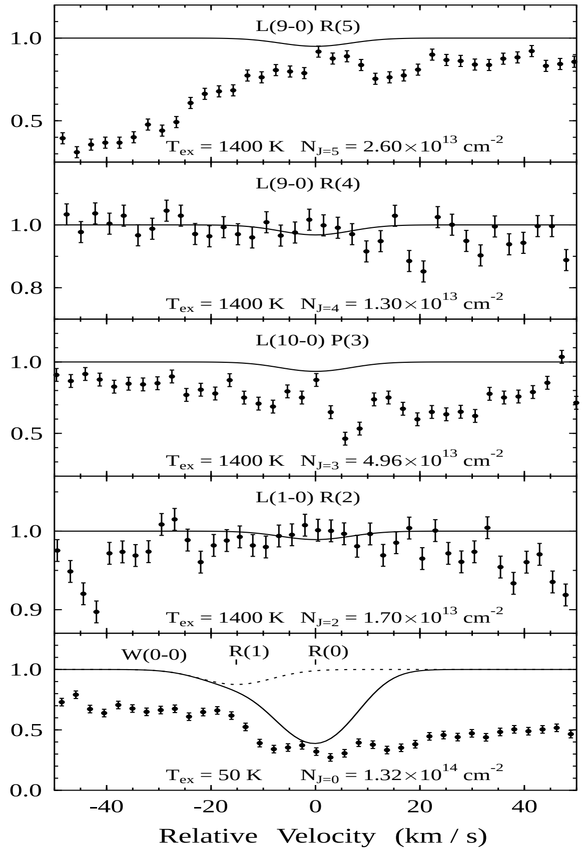

Fig. 4. Velocity plots of the UVES normalized data of Q0000–2620 (dots and 1σ error bars) obtained by Molaro et al. (2000) and the synthetic H_2 spectra convolved with the instrumental resolution of FWHM = 6 km s^{-1} (solid curves), corresponding to the limits with $T_{ex} = 50$ K for $J = 0$ (bottom panel) and $T_{ex} = 1400$ K for $J = 2 - 5$. The dotted curve in the bottom panel shows the W(0-0)R(1) profile for $N_{J=1} = 3.9 \times 10^{13}$ cm^{-2}; the Doppler parameter equals $b_{H_2} = 8.8$ km s^{-1} for all synthetic spectra (see also Fig. 1a)

Fig. 3b gives additional illustrations for our procedure. Here we show the measured ($J = 1$) and estimated ($J \neq 1$) column densities against energies of the low rotational levels. Three different lines represent solutions for $T_{ex} =$ 50, 500 and 1400 K. As seen, at low T_{ex} the most sensitive are the $J = 0$ and $J = 1$ transitions, whereas at high T_{ex} the most stringent restriction is set by the populations of the $J = 2$ and $J = 4$ rotational levels.

These two regimes are shown in Fig. 4 where dots with error bars are the observed normalized intensities within the chosen windows, and the solid curves show the H_2 synthetic profiles calculated with $b_{H_2} = 8.8$ km s^{-1} and the limiting column densities listed in the corresponding panels.

If T_{ex} lies between 50 K and 1400 K, the total molecular hydrogen column density $N(H_2)$ ranges from 5.4×10^{13} cm^{-2} to 1.7×10^{14} cm^{-2} (see Fig. 5) where the lower value is obtained at $T_{ex} = 2B_v$. Thus we may set $\log N(H_2) =$ 13.98 ± 0.25. With $\log N(\text{H I}) = 21.41 \pm 0.08$ taken from Lu et al. (1996), and assuming that the molecular gas coincide with the H I (i.e. filling factor is 1), one finds $\log f(H_2) = -7.43 \pm 0.26$ or $f(H_2) \simeq 4 \times 10^{-8}$.

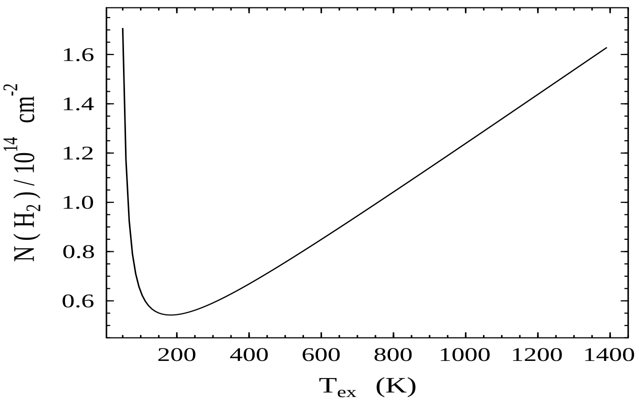

Fig. 5. The total molecular hydrogen column density $N(H_2)$ vs T_{ex} for a fixed value $N_{J=1} = 3.9 \times 10^{13}$ cm^{-2}

Since H_2 molecules are formed more efficiently on dust grains in high H I column density clouds, we can conclude that the dust number density in the $z_{abs} = 3.3901$ absorbing material is lower than in the ISM clouds with $N(\text{H I}) \gtrsim 10^{21}$ cm^{-2}, provided the dust destruction rate is the same.

2.3. Dust Content

The presence of dust in DLAs is illustrated in Fig. 6 where the relation between $\log f(H_2)$ and relative heavy element depletion, [Cr/Zn], is shown. In DLAs, the amount of dust is usually estimated from the ratio $N(\text{Cr II})/N(\text{Zn II})$ assuming that Zn is undepleted (e.g. Pettini et al. 1994).

The measured data for the four extragalactic molecular clouds (dots in Fig. 6) can be very well fitted with a linear law : $\log f(H_2) \simeq -5.5\,[\text{Cr/Zn}] - 7.1$, which means that these quantities are strongly correlated (dashed line in Fig. 6). Another four DLAs with high neutral hydrogen column densities where the H_2 absorption has not yet been detected (see Table 1) are marked by vertical arrows. Crosses in Fig. 6 are the Galactic interstellar medium measurements taken from the compilation of Roth & Blades (1995). By the horizontal lines we mark the H_2 measurements in the Magellanic Clouds (Richter 2000). Unfortunately, the corresponding [Cr/Zn] data are not available yet, therefore, to restrict their plausible range we took the limiting values of [Cr/Zn] $= -1.09$ and -0.72 obtained from different sightline measurements in the Magellanic Clouds by Roth & Blades (1997).

Qualitatively, the DLA data, including the $f(H_2)$ upper limits, exhibit the same tendency as the Galactic ISM diffuse clouds, i.e. clouds with large amount of H_2 show higher heavy element depletion. The linear correlation among the DLA systems is then a kind of upper envelope of all the different types of data points. The fact that the ISM measurements are found at higher Cr depletion than the DLA data is probably due to the higher metallicity and dust content of interstellar clouds. In fact, there is evidence for a correlation between dust-to-gas ratio and metallicity among DLA systems (Vladilo 1998). Given such a correlation, it is natural to expect that DLA points, which have lower metallicities than interstellar clouds, have also lower Cr depletion. The lack of any data points above the envelope can be readily explained because clouds with low dust content (and low Cr depletion) are expected to have low molecular content. It is interesting that the data of the Magellanic Clouds fall in the range occupied by DLAs, as expected. Indeed, typical dust-to-gas ratios in the Magellanic Clouds are about 4 times (LMC) and 8 times (SMC) lower as compared with the Milky Way (Koornneef 1982; Bouchet et al. 1985, respectively).

The fact that the DLA measurements lie on the envelope while the upper limits lie below is puzzling. One possible explanation is the presence of some selection effect that allows us to detect H_2 at high Cr depletions only when the H_2 lines are sufficiently strong. This could be the case if dust obscuration is important.

The dust number density, $n_{\rm d}$, in the $z_{\rm abs} = 3.3901$ cloud may be estimated from the measured H_2 fractional abundance assuming that the H_2 formation rate on dust grains, R, is in equilibrium with the H_2 destruction caused by UV photons. Another channel of the H_2 formation through the formation of the catalyst H^- (e.g., Donahue & Shull 1991) may compete with the dust process in the partially ionized warm regions and will not be considered here because of the very high H I column density in the $z_{\rm abs} = 3.3901$ cloud which provides most of the gas to be neutral. In the mostly neutral gas, H_2 will be in equilibrium with a density (e.g., Spitzer 1978) :

$$I\,n({\rm H}_2) = R\,n\,n({\rm H})\,, \quad (6)$$

where I is the H_2 photo-dissociation rate in s^{-1}, $n = n({\rm H}) + 2\,n({\rm H}_2)$ in cm^{-3}, and R in cm^{3}s^{-1}. For tenuous interstellar clouds, $I \simeq 0.11\,\beta_0$, with β_0 being the photo-absorption rate in the Lyman- and Werner- bands.

The H_2 formation rate on dust grains can be written as (Spitzer 1978) :

$$R\,n = \frac{1}{2}\,\langle\gamma v_{\rm H}\rangle\,\langle n_{\rm d}\sigma_{\rm d}\rangle\,, \quad (7)$$

where the constant $\gamma \simeq 0.3$, the mean thermal velocity of the H I atoms caused by particle collisions $\langle v_{\rm H}\rangle \simeq 1.46 \times 10^4\,\sqrt{T_{\rm kin}}$ in cm s^{-1}, and $\langle n_{\rm d}\sigma_{\rm d}\rangle$ is the mean area obscured by dust grains in 1 cm^3 along the sightline.

The value of β_0 depends on the local UV radiation field. The intergalactic background radiation at $z \sim 3$ gives $\beta_0 = 2 \times 10^{-12}$ s^{-1} if $J_{21}(912\,{\rm \AA}) = 1$ (Srianand & Petitjean 1998). If we take into account that locally in the intervening galaxy the UV emission from hot stars may

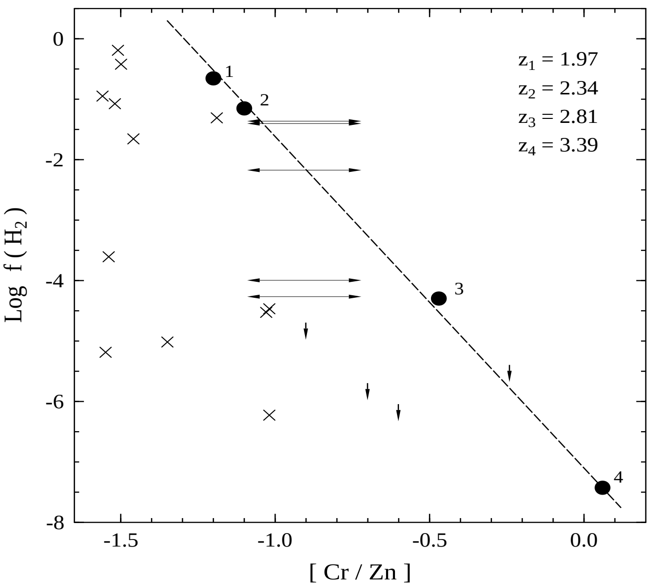

Fig. 6. Relation between H_2 fractional abundance plotted on a logarithmic scale and relative heavy element depletion in high redshift DLAs (dots, vertical arrows label systems from Table 1). The dashed line corresponds to the linear law : $\log f({\rm H}_2) \simeq -5.5\,[{\rm Cr/Zn}] - 7.1$. The same plot for the Galactic ISM diffuse clouds based on the data from the compilation of Roth & Blades (1995) are shown by crosses. The horizontal lines mark the H_2 measurements (Richter 2000) in the Magellanic Clouds (see text for details). References: 1,2 – Ge & Bechtold 1999; 3 – Levshakov & Varshalovich 1985, Srianand & Petitjean 1998; 4 – this work

increase β_0 by a factor of κ, then using (6) and (7) we have an estimate

$$\langle n_{\rm d}\sigma_{\rm d}\rangle = 5.0 \times 10^{-17}\frac{\kappa}{\sqrt{T_{\rm kin}}}\,f({\rm H}_2)\,, \quad (8)$$

where we took $n({\rm H}_2)/n({\rm H}) = N({\rm H}_2)/N({\rm H\,I})$ which is valid for the Q0000–2620 cloud.

Given the mean Galactic value $\langle n_{\rm d}\sigma_{\rm d}\rangle_{\rm ISM} = 1.2 \times 10^{-21}$ cm^{-1} (Spitzer 1978), one has

$$\frac{\langle n_{\rm d}\sigma_{\rm d}\rangle_{\rm DLA}}{\langle n_{\rm d}\sigma_{\rm d}\rangle_{\rm ISM}} = 4.0 \times 10^4\frac{\kappa}{\sqrt{T_{\rm kin}}}\,f({\rm H}_2)\,. \quad (9)$$

If $\kappa/\sqrt{T_{\rm kin}} \sim 1$ and the linear size distribution function for the dust grains is invariant, then for the $z_{\rm abs} = 3.3901$ cloud the last relation yields $\langle n_{\rm d}\rangle_{\rm DLA}/\langle n_{\rm d}\rangle_{\rm ISM} \sim 10^{-3}$.

It is reasonable to compare this quantity with the dust-to-gas ratio, $\tilde{k}$, which may be estimated from any two elements X and Y having similar nucleosynthetic history (cf. Vladilo 1998) :

$$\tilde{k} = \frac{10^{[{\rm X/H}]_{\rm obs}}}{f_{\rm X,ISM} - f_{\rm Y,ISM}}\left(10^{[{\rm Y/X}]_{\rm obs}} - 1\right)\,, \quad (10)$$

where the fraction in dust $f_{\rm X,ISM}$ refers to the Galactic interstellar medium.

By applying error propagation to the column density measurements for the Fe IIλ1611, Cr IIλ2056, and Zn IIλ2026 lines (Table 1 in Paper I), one can find that [Fe/Zn] = 0.03 ± 0.07 and [Cr/Zn] = 0.05 ± 0.08. Equation (10) implies that positive values of the [Fe/Zn] and [Cr/Zn] ratios are unphysical because of the dust depletions $f_{\rm Zn,ISM} = 0.35$, $f_{\rm Cr,ISM} = 0.92$, and $f_{\rm Fe,ISM} = 0.94$. Therefore we can estimate only maximum value of $\tilde{k}$ taking low bounds of [Fe/Zn] = -0.04 and [Cr/Zn] = -0.03, and the upper bound of [Zn/H] = -1.97. Under these conditions we have $\tilde{k} \leq 1.6 \times 10^{-3}$. This value corresponds precisely to the dust number density ratio estimated above from the H_2 fractional abundance. The same result implies that the current interpretation of the Cr/Zn ratios as due to differential dust depletion rather than intrinsic chemical abundance differences of Zn, as claimed by several authors, is correct.

3. Future Prospects

The accuracy of the estimated physical parameters $N(H_2)$ and $T_{\rm ex}$ may be improved by additional observations of the quasar 0000–2620 to increase the signal-to-noise ratio at the expected positions of the L(1-0)R(2) and L(9-0)R(4) lines where we observe rather narrow ($|\Delta v| \lesssim 15$ km s^{-1}) continuum windows free from the Lyα forest contaminations (see Fig. 4). At some level of S/N one may detect weak absorption features corresponding to these H_2 transitions. For the measured ortho-H_2 column density $N_1 = 3.9 \times 10^{13}$ cm^{-2}, such detection at 3σ level becomes possible starting from S/N $\simeq 60$, if $T_{\rm ex} \gtrsim 10^3$ K (see Table 2). The S/N ratios listed in Table 2 were estimated in the following way.

For weak absorption lines ($\tau_0 \ll 1$) one has (see LCFB) :

$$W \simeq 8.85 \times 10^{-18} \, N \, \lambda_0^2 \, f_{\rm abs} \, , \qquad (11)$$

where the equivalent width W is given in mÅ, N in cm^{-2}, and λ_0 in Å.

The equivalent width detection limit, $\sigma_{\rm lim}$, defined in LCFB, depends on the spectral resolution, the mean S/N value per pixel and the accuracy of the continuum fit, $\sigma_{\rm c}/C$, over the width of the line :

$$\sigma_{\rm lim} = \Delta\lambda \left[\left(\frac{S}{N}\right)^{-2} \mathcal{M} + \left(\frac{\sigma_{\rm c}}{C}\right)^2 \mathcal{M}^2 \right]^{1/2} , \qquad (12)$$

where $\mathcal{M} = 2.5\times$FWHM is the full width (in pixels) at the continuum level of a weak absorption line, and $\Delta\lambda$ is the pixel size in Å.

For real data, $\sigma_{\rm c}/C < ({\rm S/N})^{-1}$ since the continuum level is usually estimated as a mean intensity over m pixels within a continuum window. Thus we may write $\sigma_{\rm c}/C = \xi({\rm S/N})^{-1}$, where $\xi \simeq 1/\sqrt{m}$. Then from (12) we have

$$\frac{\rm S}{\rm N} = \frac{\Delta\lambda}{\sigma_{\rm lim}} \left[\mathcal{M}(1 + \xi^2 \mathcal{M}^2 \right]^{1/2} . \qquad (13)$$

Table 1. QSO candidates for H_2 absorption

QSO	$z_{\rm abs}$	N(H I), cm^{-2}	[Cr/Zn]	$f^a(H_2)$	$f^b(H_2)$
0458–02	2.04	8.0(21)	−0.7	< 2.0(−6)	5.0(−4)
0100+13	2.30	2.5(21)	−0.24	< 4.0(−6)	1.6(−6)
0112+03	2.42	1.0(21)	−0.9	< 2.0(−5)	6.3(−3)
1223+17	2.47	3.0(21)	−0.6	< 9.0(−7)	1.6(−4)

[a] Upper limits from Ge & Bechtold (1999)
[b] Estimated from $\log f(H_2) = -5.5\,[{\rm Cr/Zn}] - 7.1$

Table 2. Predicted equivalent widths for the L(1-0)R(2) and L(9-0)R(4) lines for different $T_{\rm ex}$ and the S/N ratios which can provide 3σ level detection

$T_{\rm ex}$ (K)	$N_{J=2}$ (cm^{-2})	$N_{J=4}$ (cm^{-2})	$W^{\rm obs}_{\rm R(2)}$ (mÅ)	$W^{\rm obs}_{\rm R(4)}$ (mÅ)	S/N R(2)	S/N R(4)
1400	1.70(13)	1.30(13)	2.90	7.97	165	60
1000	1.54(13)	8.39(12)	2.63	5.14	180	90
500	1.09(13)	1.80(12)	1.86	1.10	260	430

In our calculations we set $\Delta\lambda = 0.04$ Å, FWHM = 2.5 pixels, and $\xi = 0.2$. After that we calculate $N_{J=2}$ and $N_{J=4}$ using (5) for a given $T_{\rm ex}$ and the corresponding W values from (11). Taking $\sigma_{\rm lim} = \frac{1}{3}W$, we find S/N values from (13). The obtained results listed in the sixth and seventh columns of Table 2 show that the L(1-0)R(2) and/or L(9-0)R(4) lines may be detected for a reasonable exposure time if $T_{\rm ex}$ is not very low in the $z_{\rm abs} = 3.3901$ absorbing cloud.

Another issue we would like to outline in this section is the DLAs with N(H I) $\geq 10^{21}$ cm^{-2} and $z_{\rm abs} > 2$ from the compilation of Ge & Bechtold (1999). These systems are listed in Table 1. Similar to our case, they show high neutral hydrogen column densities but no H_2 absorption in moderate resolution spectra (FWHM $\simeq 1$ Å). The upper limits for $f(H_2)$ are shown in the fifth column of Table 1. In the sixth column we present the expected $f(H_2)$ values based on the linear relationship between $\log f(H_2)$ and [Cr/Zn] as found in this paper. As noted in Sec. 2.3, it is surprising that there is only one DLA system ($z_{\rm abs} = 2.30$) which is consistent with our results, i.e. the predicted H_2 fractional abundance is lower than the previously obtained upper limit. All other systems show too low limits for $f(H_2)$ to be in concordance with expected values.

One may advocate an intrinsic spread of the H_2 fractional abundance among DLAs at constant [Cr/Zn] ratios as an explanation. It would be also necessary to investigate the sample of QSOs of Table 1 with data of similar resolution and S/N ratios than the one presented here. Such studies could help us to understand the dust formation history and the metal enrichment of damped QSO systems since dust is mainly produced in the cool envelopes of intermediate-mass stars and in the dense shells of supernova remnants.

4. Conclusions

The outcome of our study, aiming to provide a measurement of the molecular hydrogen abundance in the low metallicity DLA galaxy at $z_{\rm abs} = 3.3901$ toward Q0000-2620, is as follows.

1. In the high resolution UVES spectrum of the quasar 0000–2620 a weak absorption feature at $\lambda_{\rm obs} = 4609.4$ Å is identified with the H_2 L(4-0)R(1) line from the $z_{\rm abs} = 3.3901$ system.

2. The application of the standard Voigt fitting analysis to this line gives the ortho-H_2 column density of $N_{J=1} = (3.9 \pm 0.9) \times 10^{13}$ cm^{-2} and the Doppler width $b_{\rm H_2} = 8.8^{+3.0}_{-0.8}$ km s^{-1}. The width of the H_2 line is found to match those for numerous unsaturated metal lines measured at the same redshift in Paper I.

3. The upper limits to the column densities of the W(0-0)R(0)+R(1), L(1-0)R(2), L(10-0)P(3), L(9-0)R(4), L(9-0)R(5) lines together with the measured value of $N_{J=1}$ lead to the excitation temperature $T_{\rm ex}$ ranging from 50 K to 1400 K.

4. The range of $T_{\rm ex}$ and the $N_{J=1}$ value yield, in turn, the total H_2 column density of $N(\mathrm{H_2}) \simeq (0.5 - 1.7) \times 10^{14}$ cm^{-2} and the H_2 fractional abundance of $f(\mathrm{H_2}) \simeq 4 \times 10^{-8}$. This is the lowest H_2 fractional abundance ever measured.

5. Assuming that the H_2 formation rate on dust grains is in equilibrium with the H_2 destruction caused by UV photons, the dust number density is estimated in the $z_{\rm abs} = 3.3901$ cloud, $\langle n_{\rm d}\rangle_{\rm DLA} \sim 10^{-3}\,\langle n_{\rm d}\rangle_{\rm ISM}$. This value is in excellent agreement with the dust-to-gas ratio of $\tilde{k} \leq 1.6 \times 10^{-3}$ found independently from the [Cr/Zn] and [Fe/Zn] abundance ratios.

6. The derived H_2 fractional abundance excellently fits in the linear relation between $\log f(\mathrm{H_2})$ and [Cr/Zn] measured for other DLAs at high redshift.

7. It is shown that future observations with higher signal-to-noise ratio (S/N > 60) may reveal a few additional H_2 lines from the $z_{\rm abs} = 3.3901$ system which may increase the accuracy of the $N(\mathrm{H_2})$ and $T_{\rm ex}$ measurements.

Acknowledgements. We are deeply indebted to the people involved in the realization of the UVES spectrograph which made possible to achieve the results presented here. We also thank an anonymous referee for his/her comments. The work of S.A.L. is supported by the RFBR grant No. 00-02-16007.

References

Bechtold J. 1999, in 'H_2 in Space', eds. F. Combes, G. Pineau des Forets (Cambridge University Press, Astrophys. Ser.), in press
Bouchet P., Lequeux J., Maurice E., Prevot L., Prévot-Burnichon M. L. 1985, A&A 149, 330
de Bruyn A. G., O'Dea C. P., Baum S. A. 1996, A&A 305, 450
Carilli C. L., Lane W., de Bruyn A. G., Braun R., Miley G. K. 1996, AJ 111, 1830
Dalgarno A. 1976, in Frontiers of Astrophysics, ed. E. H. Avrett (Harvard University Press), p.371
Dekker H., D'Odorico S., Kaufer A., Delabre B., Kotzolwski H. 2000, in Proceedings of the SPIE 4008, in press
Donahue M., Shull J. M. 1991, ApJ 383, 511
Ge J., Bechtold J. 1997, ApJ 477, L73
Ge J., Bechtold J. 1999, in 'Highly Redshifted Radio Lines', ASP Conf. Ser. 156, eds. C. L. Carilli, S. J. E. Radford, K. M. Menten, G. I. Langston, p. 121
Ge J., Bechtold J., Kulkarni V. 2000, ApJ, submit.
Koornneef J. 1982, A&A 107, 247
Levshakov S. A., Varshalovich D. A. 1985, MNRAS 212, 517
Levshakov S. A., Chaffee F. H., Foltz C. B., Black J. H. 1992, A&A 262, 385 [LCFB]
Lu L., Sargent W. L. W., Barlow T. A., Churchill C. W. 1996, ApJS 107, 475
Lu L., Sargent W. L. W., Barlow T. A. 1999, in 'Highly Redshifted Radio Lines', ASP Conf. Ser. 156, eds. C. L. Carilli, S. J. E. Radford, K. M. Menten, G. I. Langston, p. 132
Molaro P., Bonifacio P., Centurión M., D'Odorico S., Vladilo G., Santin P., Di Marcantonio P. 2000, ApJ, in press, astro-ph/0005098 [Paper I]
Morton D. C., Dinerstein H. L. 1976, ApJ 204, 1
Pettini M., Smith L. J., Hunstead R. W., King D. L. 1994, ApJ 426, 79
Richter P. 2000, A&A, in press, astro-ph/0005266
Roth K. C., Blades J. C. 1995, ApJ 445, L95
Roth K. C., Blades J. C. 1997, ApJ 474, L95
Savage B. D., Bohlin R. C., Drake J. E., Budich W. 1977, ApJ 216, 291
Savaglio S., Cristiani S., D'Odorico S., Fontana A., Giallongo E., Molaro P. 1997, A&A 318, 347
Spitzer L., Jr. 1978, Physical Processes in the Interstellar Medium (NY: Wiley-Interscience)
Spitzer L., Jr., Jenkins E. B. 1975, ARA&A 13, 133
Srianand R., Petitjean P. 1998, A&A 335, 33
Vladilo G. 1998, ApJ 493, 583